Investigation on Nonlinearity of Vertical Wave Bending Moment Based upon CFD

Kei SUGIMOTO*, Yuki YOSHIDA**

1. INTRODUCTION

Vertical wave bending moment is one critical factor in hull structure design, and appropriate consideration of this moment is essential. In classification society's rules, the Unified Requirements (URS11 and UR S11A) and Common Structural Rules (CSR) of the International Association of Classification Societies (IACS) specify the vertical wave bending moment, and formulate the maximum value (maximum hogging moment) and minimum value (maximum sagging moment) of the vertical bending moments that occur during the design life of the ship [1], [2], [3]. In addition to the maximum expected value (e.g., value of the 10^{-8} probability of exceedance) obtained based on the linear theory, these formulae also take into account, either explicitly or implicitly, the nonlinear effects that occur under large wave heights, as well as the effects of maneuvering. Among these, focusing on nonlinear effects, nonlinear effects are formulated explicitly in UR S11A, which was developed in recent years, but these rules are limited to container ships, and in UR S11, which was developed prior to UR S11A, those effects are not clearly specified.

Various research results in connection with nonlinear effects have been reported. However, if those effects are classified in several levels, Computational Fluid Dynamics (CFD) is positioned as a "Fully Nonlinear" computational technique [4], [5], and its effectiveness has been reported [6], [7], [8], particularly in studies that consider slamming impact forces and green water loads, and in evaluations of whipping elastic vibration by coupled structural analysis. However, when estimating the 10^{-8} maximum expected value, it is necessary to perform calculations equivalent to 1 000 waves, even assuming that the expected value is roughly equal to the 10^{-3} maximum expected value in the most severe short-term sea state [9]. Thus, from the viewpoint of computational time, it would be particularly difficult to apply this approach in applications that examine the nonlinear effects of diverse ships within a practical timeframe.

As methods that consider practicality and reduce computational costs, several techniques which estimate the wave profile that makes the largest contribution to responses have been proposed, and as one such methods, several design irregular wave methods have been proposed [10], [11], [12], [13]. Dietz proposed the Most Likely Response waves (MLRW) for the estimation of the maximum expected value of the vertical wave bending moment of container ships, and showed that the results of a direct time-series calculation corresponding to the probability of exceedance and the results of a calculation using the MLRW are in good agreement [12].

Therefore, in this research, trial calculations of the nonlinearity of vertical wave bending moments that can occur in the extreme sea states considered in hull structural design were carried out for a total of 55 ships by using CFD, which is an advanced analytical technique, and giving wave conditions for a design irregular wave MLRW, and the tendencies and other features of the obtained vertical bending moments were considered.

2. IACS UNIFIED REQUIREMENTS (UR)

2.1 IACS UR S11

In IACS UR S11 (Rev. 10, 2020) and IACS CSR B&T (2023), the vertical wave bending moments (hogging $M_{WV\text{-}Hog}$ and sagging ($M_{WV\text{-}Sag}$) are given by the following formulae [1], [2]:

* Research Institute, Research and Development Division, ClassNK
** Rule Development Department, Research and Development Division, ClassNK

$$M_{WV-Hog} = +190 MCL^2 BC_b \times 10^{-3} \quad (kN \cdot m)$$
$$M_{WV-Sag} = -110 MCL^2 B(C_b + 0.7) \times 10^{-3} \quad (kN \cdot m) \tag{1}$$

where, L is the ship length, B is breadth, and C_b is the block coefficient. C is a coefficient specified corresponding to the length of the ship, and M a distribution factor expressing the distribution along the ship length, and is 1.0 around midship.

The difference between the formulae for hogging and sagging occurs because the nonlinearity of sagging moment is considered. Accordingly, if it is assumed hypothetically that hogging is linear equivalent, this means that a nonlinear effect of $110 (C_b + 0.7) / (190 C_b)$ occurs in sagging moment.

2.2　IACS UR S11A

Next, among the said bending moments specified in IACS UR S11A (2015), those of the midship section are given by the following formulae [3]:

$$M_{WV-Hog} = +1.5 f_R L^3 CC_w \left(\frac{B}{L}\right)^{0.8} f_{NL-Hog} \quad (kN \cdot m)$$
$$M_{WV-Sag} = -1.5 f_R L^3 CC_w \left(\frac{B}{L}\right)^{0.8} f_{NL-Sag} \quad (kN \cdot m) \tag{2}$$

$$f_{NL-Hog} = 0.3 \frac{C_b}{C_w} \sqrt{T}$$
$$f_{NL-Sag} = 4.5 \frac{1+0.2 f_{Bow}}{C_w \sqrt{C_b} L^{0.3}} \tag{3}$$

where, C_W is waterplane area coefficient, and f_R is a factor related to the operational profile and is to be taken as 0.85. f_{NL-Hog} and f_{NL-Sag} are nonlinear correction factors for hogging and sagging moments, respectively, and depend on C_b, C_w, and T (scantling draught). In the case of sagging, the vertical bending moment is formulated including a bow flare shape coefficient (f_{Bow}) to take into account differences in the pressure-receiving area of the bow. With the exceptions of f_R and $f_{NL-Hog/Sag}$, the formulae are equivalent to the 10^{-8} values. In addition to the above, formulae are also provided for distribution of the vertical wave-induced bending moments along the ship's length. Although the product of formula (2) multiplied by 1.0 is considered for around midship, it is characteristic feature that the range is different for hogging and sagging.

3.　TARGET SHIPS OF CALCULATIONS

The target ships of the calculations were a total of 55 vessels of various types, including bulk carriers, oil tankers, and container ships. Each vessel was modeled for the Full load condition and the Ballast condition (i.e., total of 110 models). Fig. 1 shows the principal particulars of the target ships. The plots of the red circles in Fig. 1 show CSR-applied ships, blue shows container ships, and the remainder indicate other types of ships. _slender and _blunt mean $C_b < 0.7$ and $C_b \geq 0.7$, respectively. It should be noted that the parameters C_b, C_W, and T, etc. in the figure are not values defined by the rules (i.e., not scantling draught-based values), but rather, the values used in the computational models. In the following, C_b, C_W, and T are different between Full load condition and Ballast condition.
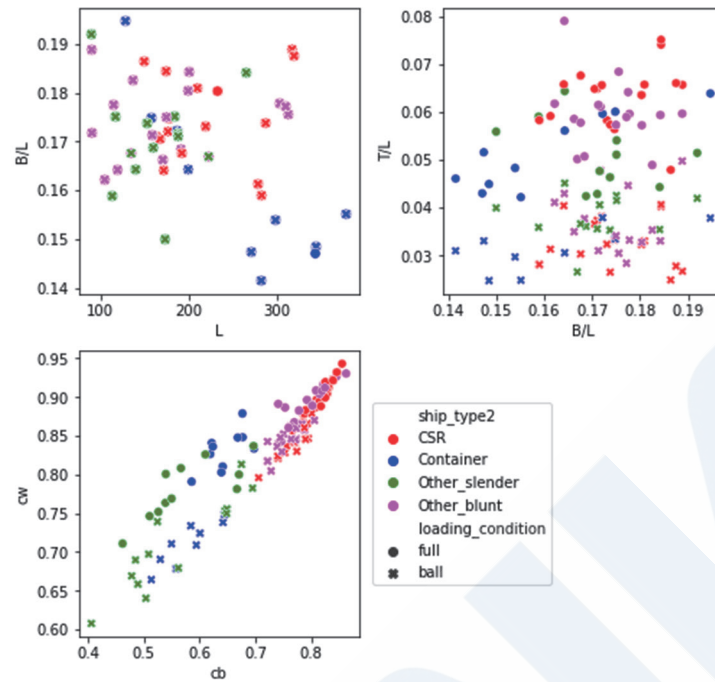
Fig. 1   Principle particular of target ships (circles: Full load condition, crosses: Ballast condition)

4.   NUMERICAL SIMULATIONS BY DESIGN IRREGULAR WAVE AND CFD

4.1   Analysis Program

In order to construct the dataset (Response Amplitude Operator, RAO, and phase difference) necessary in identification of the sea state conditions described in the following and creation of the design irregular wave, a linear load analysis program (3DPM.L) developed by the Society employing a 3-dimensional Green's function approach [14] was used. In the prepared design irregular wave MLRW, the commercial CFD program, Simcenter STAR-CCM+ 2210 [15], was used to reproduce vertical bending moments including nonlinear effects.

4.2   Flow

The flow shown in Fig. 2 was used in calculating the vertical bending moments in large waves height. In this study, we focused on reproduction of the vertical bending moments that occur under short-term sea state equivalents considered in the IACS UR described in Chapter 2.
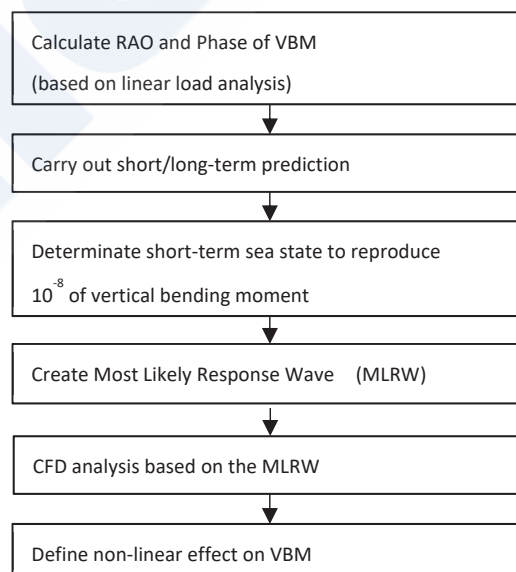

Fig. 2   Flowchart to reproduce vertical wave bending moment in extreme seas
and define non-linear effect on the moment

4.3 Sea State Conditions Considered

As the sea state conditions, the North Atlantic wave spectrum and scatter diagram specified in IACS Recommendation No. 34 (2022) were used [16), 17)]. Based on the RAO of the vertical bending moments of the target ships obtained using that information and 3-DPM.L, the 10^{-8} values were found by statistical predictions for each ship, and the target values in the design irregular wave described below were set.

A ship speed of 5 knots was used in the calculations of RAO.

4.4 Design Irregular Wave

The vertical bending moment η (t) was associated with the wave ζ (t) according to formulae (4) and (5) based on the dataset of the RAO and the phase differences of the vertical bending moments obtained by the analysis by 3-DPM.L.

$$\zeta(t) = \sum_{n=1}^{N} a_{\zeta,n}^{e}[V_n \cos(-\omega_{e,n}t) + W_n \sin(-\omega_{e,n}t)] \quad (4)$$

$$\eta(t) = \sum_{n=1}^{N} a_{\eta,n}^{e}[V_n \cos(-\omega_{e,n}t + \theta_{\eta,n}^{e}) + W_n \sin(-\omega_{e,n}t + \theta_{\eta,n}^{e})] \quad (5)$$

where, $a_{\zeta,n}^{e}$ is the wave amplitude, $a_{\eta,n}^{e}$ is the amplitude of the response, $\omega_{e,n}$ is frequency, $\theta_{\eta,n}^{e}$ is the phase difference of the response, V_n and W_n are random numbers that follow a standard normal distribution. The superscript e expresses the condition of encounter between the wave and the ship. The amplitudes of the wave and the response are expressed by $\sqrt{2S(\omega_{e,n})\Delta\omega_{e,n}}$ ($\Delta\omega_{e,n}$: difference of $\omega_{e,n}$) using their respective spectra $S(\omega_{e,n})$.

Next, the set of the Conditional Random Response Waves (CRRWs) which cause responses that satisfy the condition shown by formula (6) (magnitude of response at time $t = 0$: a_η, response: maximum or minimum, instantaneous frequency of response: ω_η) is obtained, and the MLRW is characterized by the average of the set.

$$\zeta(t) \mid_{a_\eta, \omega_\eta} \equiv \hat{E}\left[\zeta(t) \mid \eta(0) = a_\eta, \dot{\eta}(0) = 0, \frac{\dot{\hat{\eta}}(0)}{\hat{\eta}(0)} = \omega_\eta\right] \quad (6)$$

where, a_η is the magnitude of the targeted vertical bending moment, ω_η is the instantaneous frequency of the moment, $\hat{E}[\cdot|\cdot]$ is the conditional average, $\dot{\eta}(t)$ is the time derivative of the response, and $\hat{\eta}(t)$ is the Hilbert transform of the response. a_η is the value at midship section. ω_η is given by m_1/m_0 (m_n: n-th moment of the response spectrum). If m_n is the moment of a wave spectrum, this is a quantity which is equivalent to the mean wave angular frequency ($2\pi/T_{m01}$) [18)]. The analytical expressions of CRRW and MLRW are known when ω_η is given in this manner [12), 19), 20)]. The wave direction of MLRW in all the target ships was fixed as a head sea (180°).

As an example, Fig. 3 shows the associated wave $\zeta(t)$ (Fig. 3, top) and vertical bending moment $\eta(t)$ (bottom) for the hogging moment of a bulk carrier (hereinafter, BC-10) having L = abt. 290 m in the Full load condition. In the top part of the figure, the gray lines indicate a group 25 CRRW waves, the green line shows one wave in that group, and the red line shows the mean of the 25 waves. In the same figure, the blue line (MLRW) and the red line (mean of CRRW) diverge due to the limited number of CRRW waves. However, if the number of waves is increased sufficiently, the red line will converge with the blue line. In the obtained MLRW, a peak of the wave height exists at midship when $t = 0$. Therefore, the phases of the elementary waves in the wave spectrum of the MLRW were arranged using the encountered wave number, and the CFD simulation was started from the smooth water state. Furthermore, because the MLRWs at which hogging and sagging moments showed their largest values were those when the positive and negative wave height were transposed, two calculations were performed in the CFD analysis for those MLRWs.

4.5 Setting in CFD

On the assumption that fluids are incompressible, the Reynolds-averaged Navier-Stokes equation (RANS), which is the governing equation for flows, was discretized by the finite volume method. The advective term was discretized using a second-order accurate upwind difference scheme, and a backward difference scheme was used in time evolution. The Semi-Implicit Method for Pressure-Linked Equation (SIMPLE) algorithm was used as a solution for the discretization equations.

Considering a gas-liquid two-phase system consisting of air and seawater, the gas-liquid interface was obtained by using High Resolution Interface Capture (HRIC) [21], which is based on the Volume of Fluid (VOF) method.

The hull was assumed to be a rigid body, and the hull momentum was obtained by solving equations of motion for translation and rotation at the center of gravity. As the degrees of freedom of motion, only heave and pitch were considered, and others were fixed. Node movement of the fluid region surrounding the hull accompanying hull motion was performed by morphing, and the amount of node movement was determined based on Radial Basis Functions (RBF).

The MLRW was given as the inflow condition., and the Euler Overlay Method (EOM) [22] was used to prevent the influence of reflection of the wave at the interface of the computational region.

To perform calculations for a diverse range of ship types in a unified manner, the size of the computational region, mesh size, time step, etc. were given by the principal particulars of the ships (L, B, T, D (moulded depth)) and the sea state conditions (H_s (significant wave height), T_z (zero upcross wave period)).

Assuming the symmetry of the phenomena, only the half-breadth of the ships was modeled. The total number of cells was about 1×10^6 to 1.2×10^6. The simulations were begun from the smooth-water state and performed for an actual time of 50 to 70 seconds, until the peak of the wave height of the MLRW passed through the hull.

It may be noted that these settings were based on research by one of the authors [8], and the validity of the analysis results has been confirmed.

Fig. 4 shows a top view (deck direction) of the wave height distribution in the initial condition for the simulation of the hogging moment of BC-10 (Full load condition). The colors red, blue, and green indicate the wave peak, wave trough, and smooth water, respectively. White area in the center shows the ship. This figure shows a symmetrical representation of two sides of the vessel, but as noted above, the actual calculation was performed for only the half-breadth side.

Similarly, Fig. 5 shows the distribution of the VOF values of BC-10 in the initial condition as seen from the ship's breadth direction (side view) for a centerline section around the bow, together with the mesh diagram. Here, the colors light blue and white represent seawater and air, respectively.
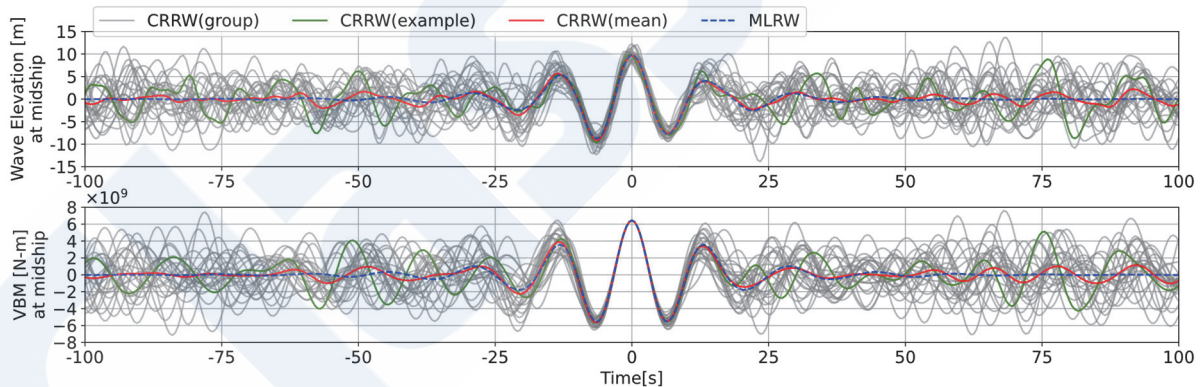

Fig. 3　An example of wave elevation and vertical bending moment in CRRW and MLRW
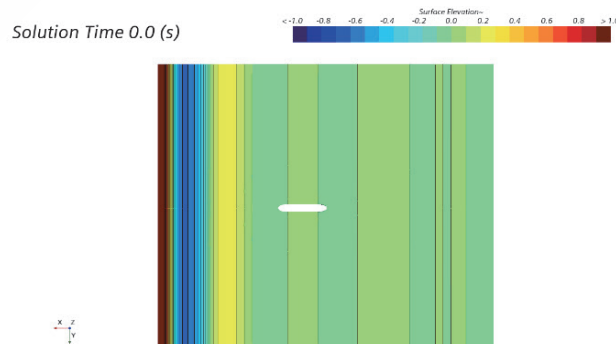(Bulk carrier, BC-10, Full load condition)

Fig. 4　Wave height distribution of BC-10 at initial condition (top view)
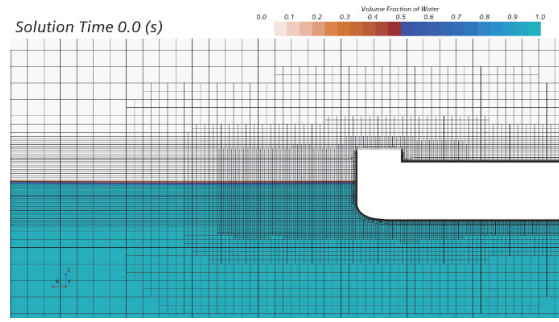
Fig. 5 VOF distribution of BC-10 with mesh diagram at initial condition (side view, near the bow)

5. SIMULATION RESULTS

5.1 Time Series, Distribution, Etc. of Vertical Bending Moment

As an example of the CFD analysis results, Fig. 6 and Fig. 7 show the results for BC-10 in the Full load condition and the Ballast condition, respectively. In order from above, (a) in Figs. 6 and 7 shows the time history of the wave elevation at midship, heave motion, the pitch motion, and the vertical bending moment in the midship section. The red line means the analysis results when targeting the hogging moment, and the blue line shows the results when targeting the sagging moment. In this example, the maximum or minimum vertical bending moment occurs at around $t = 60$ (s). The times showing the maximum value (or minimum value) are indicated by the circles in the respective times series charts.

Fig. 6 (b) and Fig. 7 (b) show the distribution of the vertical bending moment along the ship length. Here, the value of the moment in each cross section is the maximum value (or minimum value) in the respective time series. The gray lines in these figures mean the distribution of vertical bending moment obtained by linear theory, and their differences can be regarded as the nonlinear effect that occurs in the vertical bending moment in large wave heights.
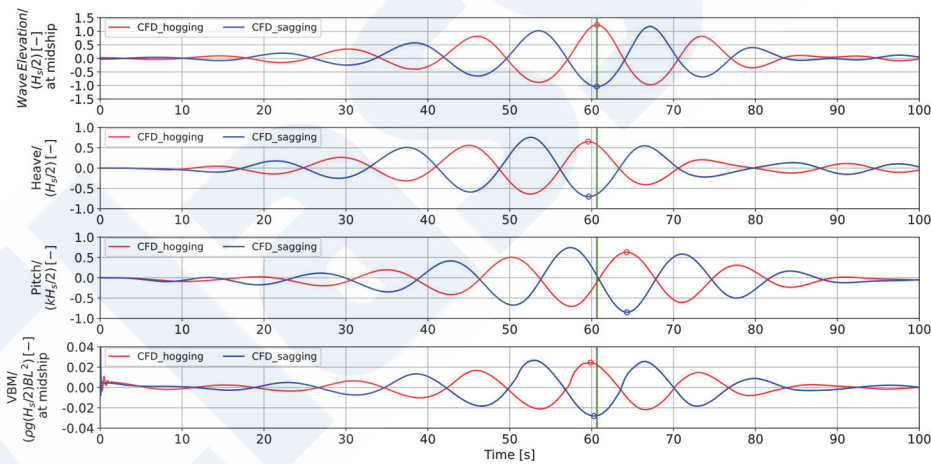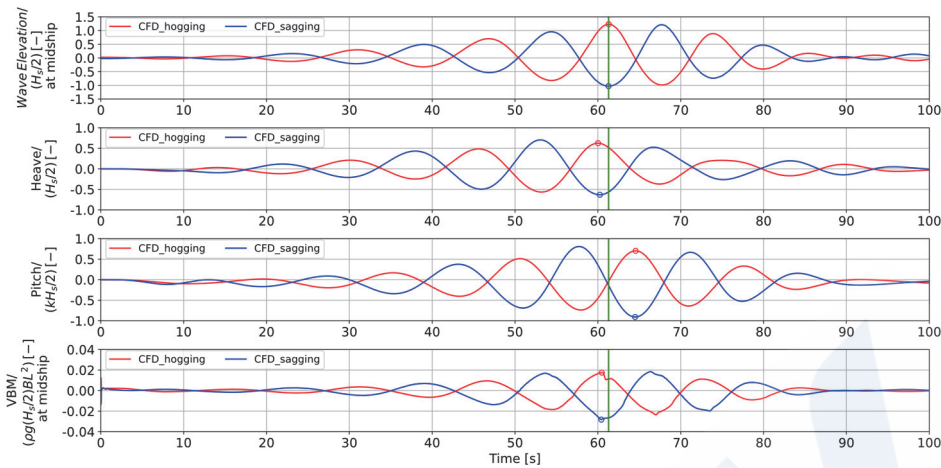

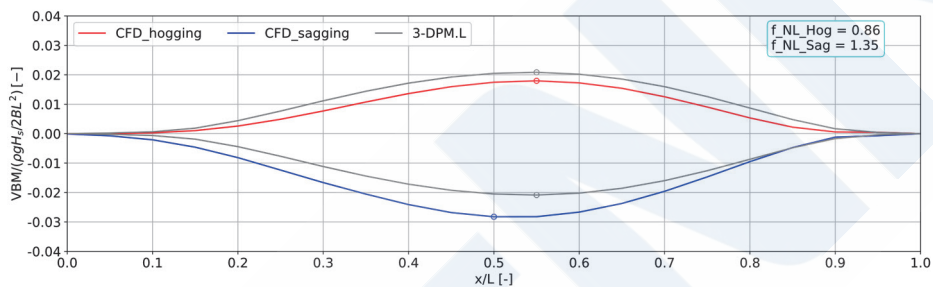(a) CFD+MLRW, Time history of wave elevation, heave, pitch and vertical bending moment
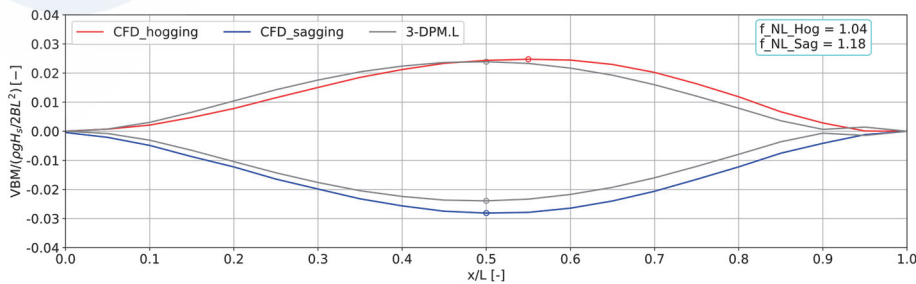
(b) CFD+MLRW, Vertical bending moment distribution along the ship length

Fig. 6 An example of CFD analysis result (Bulk carrier, BC-10, Full load condition)

(a) CFD+MLRW, Time history of wave elevation, heave, pitch and vertical bending moment

(b) CFD+MLRW, Vertical bending moment distribution along the ship length

Fig. 7　An example of CFD analysis result (Bulk carrier, BC-10, Ballast condition)

When the calculation results of the series of 55 ships (110 models) were compared, some cases showed remarkable differences in the tendency of the sagging moment, even in target ships with similar specifications. Since the results of the analysis on the effect of green water loads was suspected, a sensitivity analysis was carried out using the three forecastle shape models shown in Fig. 8 based on BC-10 (Full load condition), and the changes in the vertical bending moment were observed. Results are shown in Fig. 9. Fig. 10 shows the visualization of the green water condition in these analysis results.

The gray line in Fig. 10 indicates the relationship between the vertical bending moment based on linear theory and the probability of exceedance in the short-term sea state decided here. The red, blue, and green plots show the values of the vertical bending moments of the three forecastle shapes obtained by the CFD+MLRW analysis, and correspond to the colors in Fig. 8. Based on this, it could be understood that the sagging moment is reduced in the models in which green water acts more strongly, and it was also found that green water had no effect on hogging (although this is self-evident, because the forecastle is always exposed and green water does not act on it).

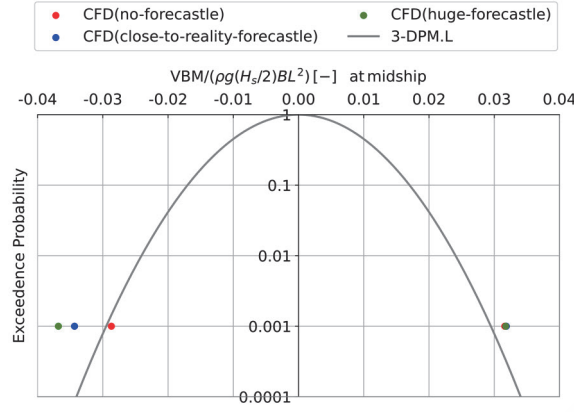Fig. 8　Side view with assumed forecastle shape model based on BC-10

Fig. 9　The effect of with/without forecastle on vertical wave bending moment at midship
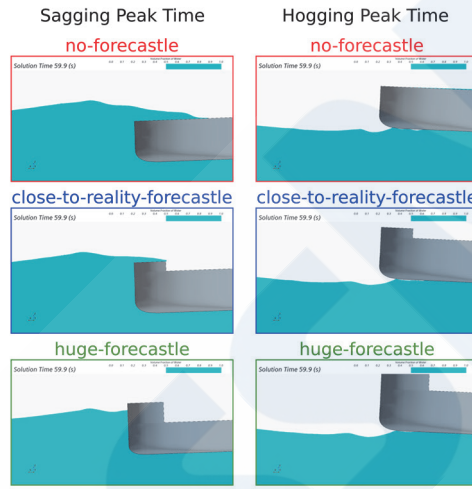(Bulk carrier, BC-10, Full load condition)

Fig. 10　Comparison of green water on deck at the time of maximum hogging and minimum sagging moment
(Bulk carrier, BC-10, Full load condition)

Based on this discussion, the calculations of the respective models in this study were unified by modeling a forecastle close to that of the real vessel. Although green water occurred in some cases, depending on the ship's draught and freeboard, visual confirmation indicated that the amount of green water was small, and in the comparative study, etc. with the principal particulars described in the following, those conditions were not sufficient to lead to a different tendency from the others. Therefore, the authors judged that it was not necessary to consider virtual cases such as the huge-forecastle in the analysis presented below.

5.2　Nonlinear Effect Coefficient and Sensitivity of Principal Particulars

In this study, the nonlinear effect of large wave heights on the vertical bending moments were defined by the formulae shown below, and are discussed in the following.

$$f_{NL-Hog} \equiv \frac{M_{WV-Hog-max}^{CFD}}{M_{WV-Hog-max}^{lienar}} = \frac{\max\limits_{0 \le x/L \le 1} M_{WV-Hog}^{CFD}(x/L)}{\max\limits_{0 \le x/L \le 1} M_{WV-Hog}^{linear}(x/L)}$$

$$f_{NL-Sag} \equiv \frac{M_{WV-Sag-min}^{CFD}}{M_{WV-Sag-min}^{linear}} = \frac{\min\limits_{0 \le x/L \le 1} M_{WV-Sag}^{CFD}(x/L)}{\min\limits_{0 \le x/L \le 1} M_{WV-Sag}^{linear}(x/L)} \tag{7}$$

where, $M_{WV-Hog-max}^{CFD}$ means the maximum value of the vertical bending moment (hogging) in the all transverse section obtained by the CFD analysis, and $M_{WV-Hog-max}^{linear}$ means the maximum value of the said moment in the all transverse section obtained by linear theory. Although the transverse section that displays the maximum value is around midship in both cases, the

two are not necessarily the same. When the subscript *min* is used, the term means sagging moment (minimum value).

Fig. 11 shows the relationship between the nonlinear effect coefficient for hogging, f_{NL-Hog}, and the principal particulars of the ships, and Fig. 12 shows the relationship between the nonlinear effect coefficient for sagging, f_{NL-Sag}, and the principal particulars of the ships. Based on these figures, it was suggested that the sensitivity for ship length L and breadth B is low, and sensitivity for the block coefficient C_b and the waterplane area coefficient C_w tends to be high. In addition, the results also confirmed that the hogging moment has the sensitivity by the draught T. Regarding the bow flare shape coefficient f_{Bow}, which is included in the nonlinear effect coefficient for the sagging moment in IACS UR S11A, a certain tendency could be observed in the container ships (see the blue plots in Fig. 12), but no clear trends could be seen in the other ships.
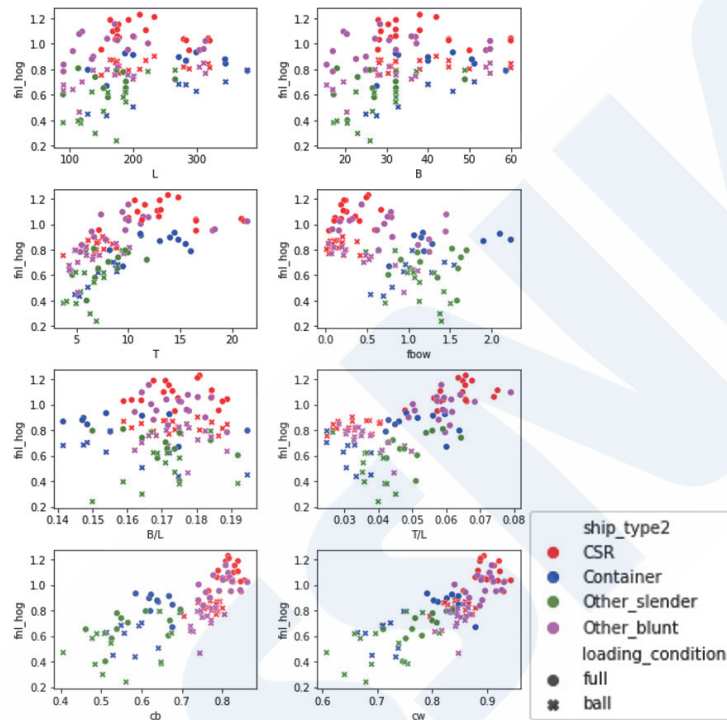

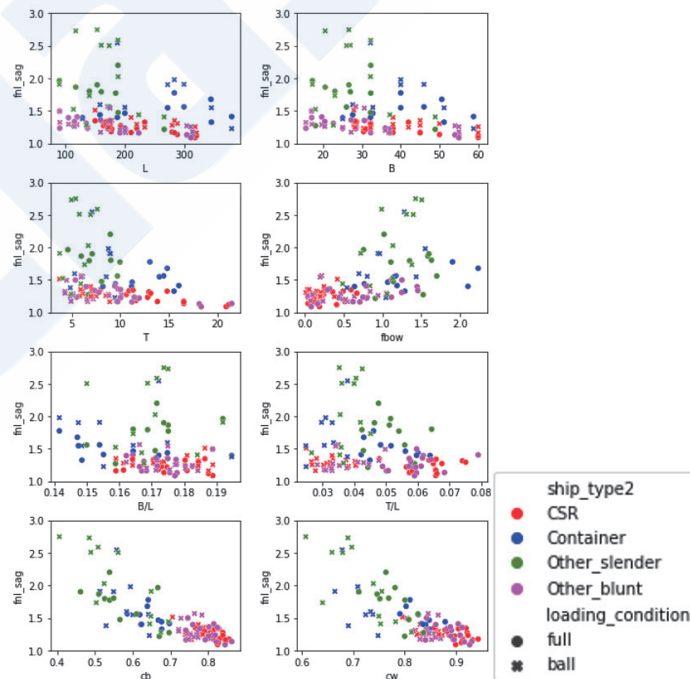Fig. 11　Sensitivity of non-linear effect coefficient to principal particulars of ships, hogging moment

Fig. 12　Sensitivity of non-linear effect coefficient to principal particulars of ships, sagging moment

5.3　Relationship between Hogging and Sagging

Fig. 13 shows the relationship between f_{NL-Hog} and f_{NL-Sag}. From the figure, the nonlinear effect is relatively small in blunt ships, and in the Full load condition, values around 1.0 were obtained in hogging and around 1.2 were obtained in sagging. In the Ballast condition, a value of around 0.8 was obtained in hogging, and a value approximately the same or very slightly larger than that in Full load condition was obtained in sagging. In slender ships, which includes container ships, it was found that the nonlinear effect in hogging was small in comparison with blunt ships, while the nonlinear effect in sagging was became relatively large.

As reference, Fig. 14 shows a comparison of the results of calculations in connection with the nonlinear effect coefficient given in a Technical background document [23] for UR S11A, which has been published by the IACS, and the results of the research presented in this paper, in the same format.

The data in Fig. 14 (b) are not CFD results, but are the results of a program based on the 3-dimensional Green's function approach, which considers nonlinearity. However, in terms of macroscopic tendencies, there are no large differences between those results and the results of this study.
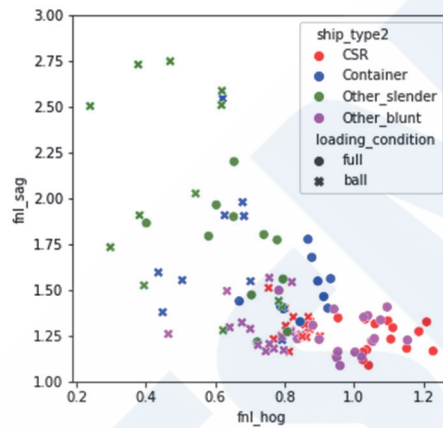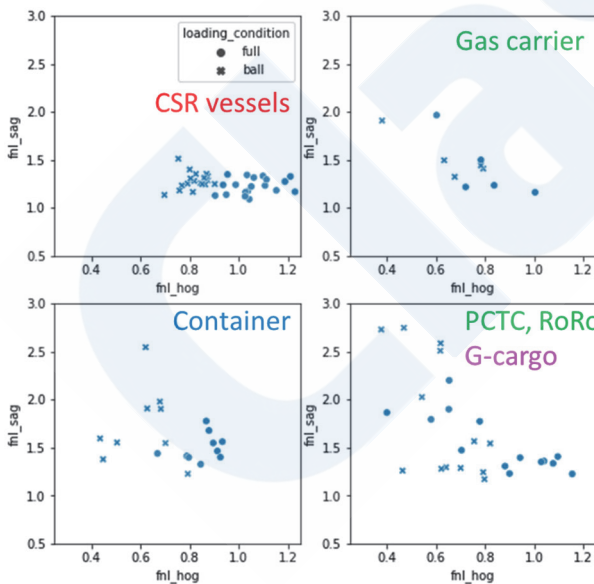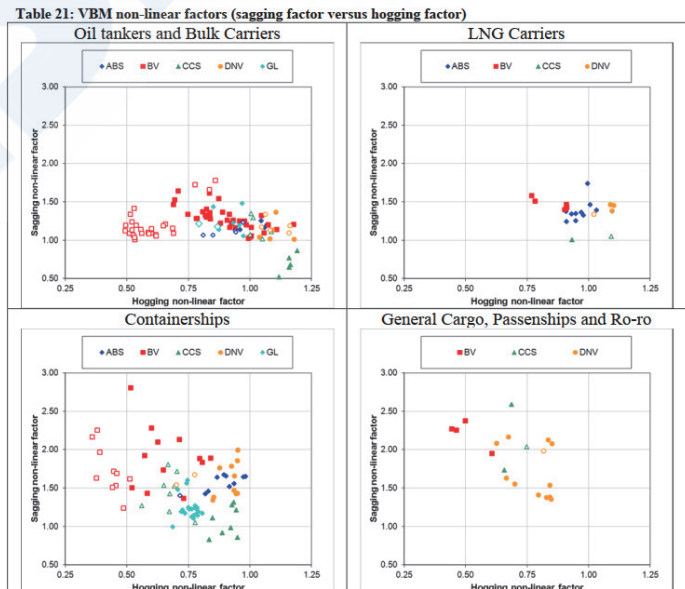

Fig. 13　Relationship between f_{NL-Hog} and f_{NL-Sag}

(a) Based on CFD+MLRW (same as Fig. 9)　　　　(b) According to an IACS document

Fig. 14　Comparison with a past investigation regarding relationship between f_{NL-Hog} and f_{NL-Sag}

Finally, Fig. 15 shows the relationship between the nonlinear effect coefficients specified in the said UR and the nonlinear effect coefficients based on the results of this study as reference. As noted in Chapter 3, the values of C_b, C_w, and T are values in the loaded condition, and the x-axis (i.e., UR values) also shows the same condition. In addition, the upper and lower limits

specified in the UR are not considered in the figure. Accordingly, this is not a strict comparison with the UR. However, from the figures, it can be thought that an approximately good correlation exists between the two. Since it is presumed that codes which consider nonlinearity based on potential theory, such as the Strip method and the 3-dimensional Green's function approach, frequently consider the nonlinearity of the Froude-Krylov force and the nonlinearity of the restoring force, which are generally considered to be dominant to nonlinear effects, the correlation shown in Fig. 15 may suggest that the effect on the nonlinearity of the vertical bending moment is small except in the case of those two components.
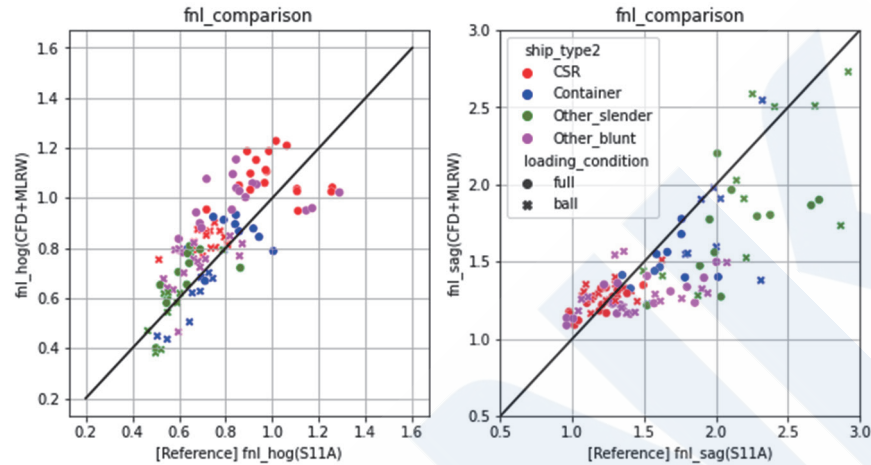

Fig. 15　Comparison with non-linear factor specified in IACS UR S11A (as reference),
(left): hogging, (right): sagging.

6.　CONCLUSION

In this study, simulations of the nonlinearity of the vertical wave bending moments that can occur in the extreme sea states considered in hull structural design were carried out for a total of 55 ships by using the advanced analytical technique CFD and giving the wave conditions by a design irregular wave.

In the trial calculation process, it was found that green sea loads are a phenomenon that suppresses the sagging moment. Therefore, modeling based on a forecastle shape close to that of the real ships was deemed essential when performing trial calculations of this phenomenon, and the simulation models were unified in that manner.

Based on the nonlinear effect coefficient defined here, the respective nonlinear effect coefficients that occur in the hogging and sagging moments were analyzed. Differences in the tendencies of blunt ships and slender ships and sensitivity to the principal particulars of the ships were observed. In addition to high tendencies with respect to C_b and C_w, a good correlation between the coefficients specified in the existing standard (IACS UR S11A) and these macroscopic tendencies was confirmed.

However, this study is ultimately only a trial calculation, and is not a comprehensive analysis of the nonlinearity that occurs in vertical bending moments. Further study is considered necessary in order to establish nonlinear effect coefficients for appropriate structural design. Examples of the issues that require further examination include study of the nonlinear effects that occur under conditions other than short-term sea states under the same calculation conditions as in this study, consideration of the nonlinear effects in following seas, and verification not only by numerical simulations for limited time domains such as MLRW, but also by a full simulation (i.e., reproduction of approximately 1 000 waves) of short-term sea states. The results of that kind of study may show that a different definition of the nonlinear effect coefficients defined in this study is appropriate. Furthermore, although linear theory was outside the scope of this study, a comprehensive study that includes terms corresponding to linear theory is also considered necessary.

REFERENCES

1)　IACS: Unified Requirement S11 Longitudinal Strength Standard, 2020.
2)　IACS: Common Structure Rules for Bulk Carriers and Oil Tankers, 2023.

3) IACS: Unified Requirements S11A Longitudinal Strength Standard for Container Ship, 2015.

4) ITTC: Recommended Procedures and Guidelines Verification and Validation of Linear and Weakly Nonlinear Seakeeping Computer Codes, 2017.

5) ISSC: Committee I.2 Loads. 18th INTERNATIONAL SHIP AND OFFSHORE STRUCTURES CONGRESS, 2012.

6) Kim, S. P.: CFD as a seakeeping tool for ship design. International Journal of Naval Architecture and Ocean Engineering, Vol. 3(1), pp.65–71, 2011.

7) Gatin, I., Vladimir, N., Malenica, Š., & Jasak, H.: Green sea loads in irregular waves with Finite Volume method. Ocean Engineering, Vol. 171, 2019.

8) J. Parunov, T. Badalotti, Q. Feng, X. Gu, K. Iijima, N. Ma, W. Qiu, S. Wang, X. Wang, P. Yang, Y. Yoshida, Z. Zhang, & C. Guedes Soares: Benchmark on the prediction of whipping response of a warship model in regular waves. Marine Structures, Vol. 94, 2024.

9) H. Mano, & H. Ueno: A Simplified Estimation of Long-Term Distributions of Various Random Variables Induced by Ocean Waves, and a Study on the Influences of Operating Conditions on the Extremes. Journal of the Society of Naval Architects of Japan, 1972(132), pp.235–247, 1972.

10) T. Fukasawa: On the Design Wave for Collapse Strength of a Ship, 9th Technical Exchange and Advisory Meeting, TEAM'95, pp.187-201, 1995.

11) Adegeest, L.J.M., Braathen, A, & Lseth, R.M.: Use of Nonlinear Sea Loads simulations in design of Ships, Proceeding of 7th PRADS, pp.53-58, 1998.

12) Dietz, JS.: Application of conditional waves as critical episodes for extreme loads on Marine Structures, Ph.D. thesis, Department of Mechanical Engineering, Technical University of Denmark, Lyngby, Denmark, 2004.

13) J. Juncher Jensen: Extreme value predictions and critical wave episodes for marine structures by FORM, Ships and Offshore Structures, 3:4, pp.325-333, 2008

14) Sugimoto, K., Fukumoto, Y., Matsuwaki J., Akamatsu, T., Ashida, S., & Onishi, K.: Non linear effect on wave induced loads for hull structural design, bulk carrier, container carrier, vehicles carrier, Proceeding of 39the international conference on ocean, offshore and arctic Engineering, 2020.

15) Siemens Digital Industries Software: Simcenter Star-ccm+ user guide version 2210, 2022.

16) IACS: Recommendation No.34, 2022.

17) Håvard, A., Guillaume, H., Michael, J., & Tingyao, Z.: Update of Wave Statistics Standards for Classification Rules, The proceeding of 9th International Conference on Marine Structures, 2023.

18) Det Norske Veritas: ENVIRONMENTAL CONDITIONS AND ENVIRONMENTAL LOADS (Recommended Practice DNV-RP-C205), 2007.

19) Drummen, I., Wu, M. K., & Moan, T.: Numerical and experimental investigations into the application of response conditioned waves for long-term nonlinear analyses. Marine Structures, Vol. 22(3), pp.576–593, 2009.

20) Quon, E., Platt, A., Yu, Y.-H., & Lawson, M.: Application of the Most Likely Extreme Response Method for Wave Energy Converters. International Conference on Ocean, Offshore and Arctic Engineering, 2016.

21) Muzaferija, S., & Peric, M.: Computation of free surface flows using interface-tracking and interface-capturing methods, Chap. 2 in O. Mahrenholtz and M. Markiewicz (eds.), Nonlinear Water Wave Interaction, Computational Mechanics Publications, WIT Press, Southampton, 1999.

22) J. Kim, J. O'Sullivan, & A. Read: Ringing analysis of a vertical cylinder by Euler overlay method, Proceedings of the International Conference on Offshore Mechanics and Arctic Engineering, OMAE2012, Vol.4, pp.855-866, 2012.

23) IACS: Technical Background of Unified Requirements S11A Longitudinal Strength Standard for Container Ship, 2015.